ACS APPLIED MATERIALS & INTERFACES

www.acsami.org Research Article

Facile Fabrication of "Tacky", Stretchable, and Aligned Carbon Nanotube Sheet-Based Electronics for On-Skin Health Monitoring

Duy Van Nguyen,* Dean Mills, Canh-Dung Tran, Thanh Nguyen, Hung Nguyen, Thi Lap Tran, Pingan Song, Hoang-Phuong Phan, Nam-Trung Nguyen, Dzung Viet Dao, John Bell, and Toan Dinh*

Cite This: *ACS Appl. Mater. Interfaces* 2023, 15, 58746−58760 Read Online

ACCESS | Metrics & More | Article Recommendations | Supporting Information

ABSTRACT: Point-of-care monitoring of physiological signals such as electrocardiogram, electromyogram, and electroencephalogram is essential for prompt disease diagnosis and quick treatment, which can be realized through advanced skin-worn electronics. However, it is still challenging to design an intimate and nonrestrictive skin-contact device for physiological measurements with high fidelity and artifact tolerance. This research presents a facile method using a "tacky" surface to produce a tight interface between the ACNT skin-like electronic and the skin. The method provides the skin-worn electronic with a stretchability of up to 70% strain, greater than that of most common epidermal electrodes. Low-density ACNT bundles facilitate the infiltration of adhesive and improve the conformal contact between the ACNT sheet and the skin, while dense ACNT bundles lessen this effect. The stretchability and conformal contact allow the ACNT sheet-based electronics to create a tight interface with the skin, which enables the high-fidelity measurement of physiological signals (the Pearson's coefficient of 0.98) and tolerance for motion artifacts. In addition, our method allows the use of degradable substrates to enable reusability and degradability of the electronics based on ACNT sheets, integrating "green" properties into on-skin electronics.

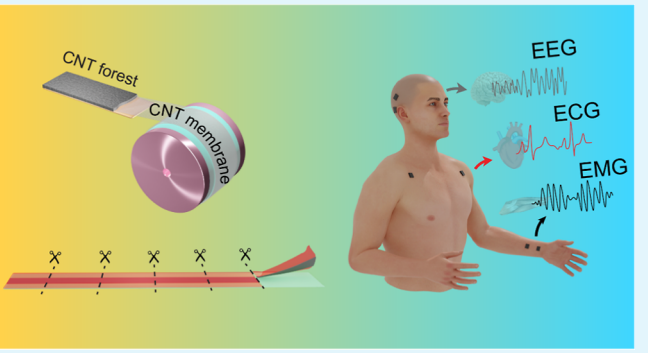

KEYWORDS: *on-skin electronics, aligned carbon nanotubes, electrophysiology, stretchability, degradability, reusability*

1. INTRODUCTION

Physiological signal monitoring has long been a basic but crucial clinical practice for the early diagnosis of fatal diseases such as atrial fibrillation, a condition that causes an abnormal heart rhythm and is a primary cause of strokes.[1] The physiological signals such as electrocardiogram (ECG), electromyogram (EMG), electroencephalogram (EEG),[2] or hemodynamic parameters[3] can be measured by laminating conductive electrodes on the skin, which is called epidermal or on-skin electronics.[4] Considering the great demand for personalized monitoring of those signals, the electrodes should be robust, long-lasting, small, thin, and lightweight to be integrated with other blocks such as amplifiers[5] or wireless communication.[6] Regarding high-quality monitoring, highly electrically conductive electrodes with skin-like mechanical properties are required to allow intimate and nonrestrictive contact with the skin surface, enabling effective coupling between the devices and the skin.[7,8] Intimate contact is essential for a larger contact area, lowering the electrical impedance of the interface between devices and the skin,[9] and for conformability that minimizes the displacement of electrodes under motion artifacts.[10] Thus, small electrodes with low contact impedance and a tight device−skin interface are highly desired.

Conventional technology utilizes "wet" electrodes (with a large skin-covering area of ∼10 cm^2) consisting of a hydrogel layer and a metal electrode to form a wet skin−electrode interface, whose sensitivity substantially decreases with dehydration. Current "dry" electrodes are typically made of bulky metals, which require skin moisture to fill the air gaps at the skin−electrode interface to achieve low impedance.[11] Therefore, it is still challenging to achieve an ultraconformal interface for artifact-tolerant sensing. Moreover, the conformal interface requires scaling down the thickness of substrates to below 5 μm (soft substrates)[9] or below 500 nm (hard substrates),[12] which results in the collapse of the electronics/electrodes after use.[13] Likewise, scaling down the thin metal films (gold) with low fracture strain (∼1%) to nanometer thickness is accompanied by the proper control of flexible shapes (such as serpentine[14]). This requires complex fabrication processes involving micro-/nanofabrication tech-

Received: September 11, 2023
Revised: November 19, 2023
Accepted: November 21, 2023
Published: December 5, 2023

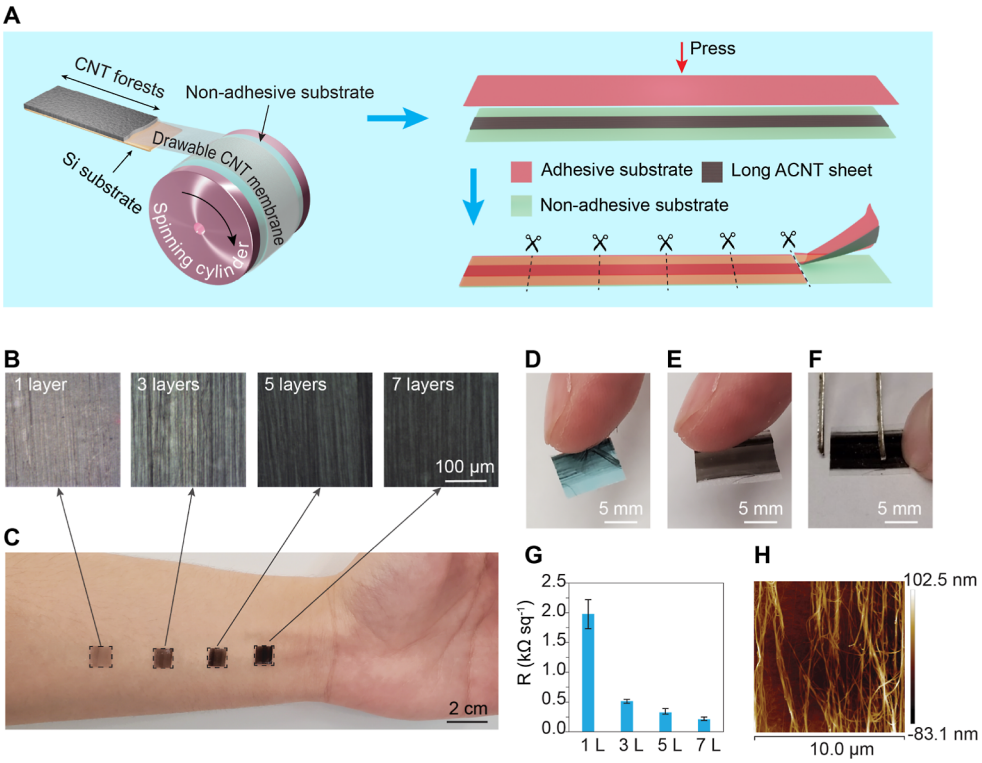

Figure 1. Fabrication and characterization of ACNT sheets. (A) Schematic illustration of the fabrication process, from drawing to transferring ACNT sheets. (B) Optical microscopy images of 1-layer, 3-layer, 5-layer, and 7-layer ACNT sheets, showing the parallel alignment of CNTs. (C) Photo of the transferred ACNT sheets on human skin. (D) Photo showing damages of an ACNT sheet before transferring. (E,F) Photos showing no visible damage of a transferred ACNT sheet after it contacted a finger or was scratched by a pair of tweezers, respectively. (G) Sheet resistance vs the number of layers of ACNT sheets (1, 3, 5, and 7 L indicate 1-layer, 3-layer, 5-layer, and 7-layer ACNT sheets, respectively). The mean values are determined by measuring the electrical resistance of the samples 4−6 times, and the maximum and minimum values are presented as error bars. (H) AFM image of a 1-layer ACNT sheet.

nologies[15,16] and the removal of materials by chemicals, cutting blades,[12,17] or laser beams[18] that potentially cause contamination to the remaining materials. Additionally, drawing conductive ink (silver flake mixed with a conductive polymer) directly on the skin can provide conformal contact for motion artifact-free sensing due to the infiltration of the ink into the creases of the skin.[10,19] However, together with the complication of the ink preparation, the repeated drawing process is low-scale and time-consuming and can cause discomfort to wearers.

Our research proposes a "tacky" approach using an adhesive surface to handle aligned carbon nanotube (ACNT) nanosheets, leading to a tight skin−sensor interface for on-skin electronics. The on-skin electrodes have a much smaller working area (~0.64 cm^2) than commercial electrodes (~4 cm^2) but still maintain a secure device−skin interface, allowing for the capture of high-quality ECG, EMG, and EEG signals and tolerance of motion artifacts. The utilization of ACNT sheets as epidermal sensors demonstrates high performance compared to that of various other on-skin sensors, including the use of random CNTs. ACNT sheets are renowned for their high electrical conductivity, excellent mechanical properties, intrinsic flexibility, chemical stability, nanometer thickness, and easy fabrication,[20−24] which makes them exceptionally well-suited for use in conformal skin-worn electronics. Working with ACNT sheets offers facile, chemical-free, cleanroom-free, and large-scale fabrication of epidermal electronics. Although there have been debates about the biocompatibility of CNTs, the recent review study by Chetyrkina et al.[25] revealed that the CNTs located on a substrate could be considered a potential conductive base for growing cells. Moreover, we have found that moderately dense ACNT bundles favor conformal skin contact with a stable and low electrical impedance of the device−skin interface, although a high density is expected to provide more contact area. The method also provides a tight interface with a large stretchability of skin-worn electrodes of up to 70% strain with an insignificant change in electrical properties. This capability satisfies the requirement of all skin applications that normally require up to 63% strain depending on body location,[7] while most common epidermal skin electrodes only work up to 30% strain[10,13,15,26] and show a large change in electrical resistance[12,27] upon stretching. Additionally, our epidermal electrodes can be reused (such as becoming strain sensors) or degraded to promote sustainability, whereas most on-skin electronics have not been reported to possess these "green" properties.[10,12−15,26−28] Therefore, our study provides valuable insights into the potential applications of diverse substrates (such as flexible, stretchable, and degradable substrates) for on-skin sensors based on ACNT sheets.

2. RESULTS AND DISCUSSION

2.1. Facile "Tacky" Methods. The fabrication process is illustrated in Figure 1A. First, we used a conventional dry-spinning method to draw an ACNT membrane from a CNT forest;[24,29] CNTs were aligned in the drawing direction (Movie S1). The membrane was stacked on a nonadhesive substrate to form 1-layer, 3-layer, 5-layer, and 7-layer ACNT

https://doi.org/10.1021/acsami.3c13541
ACS Appl. Mater. Interfaces 2023, 15, 58746−58760

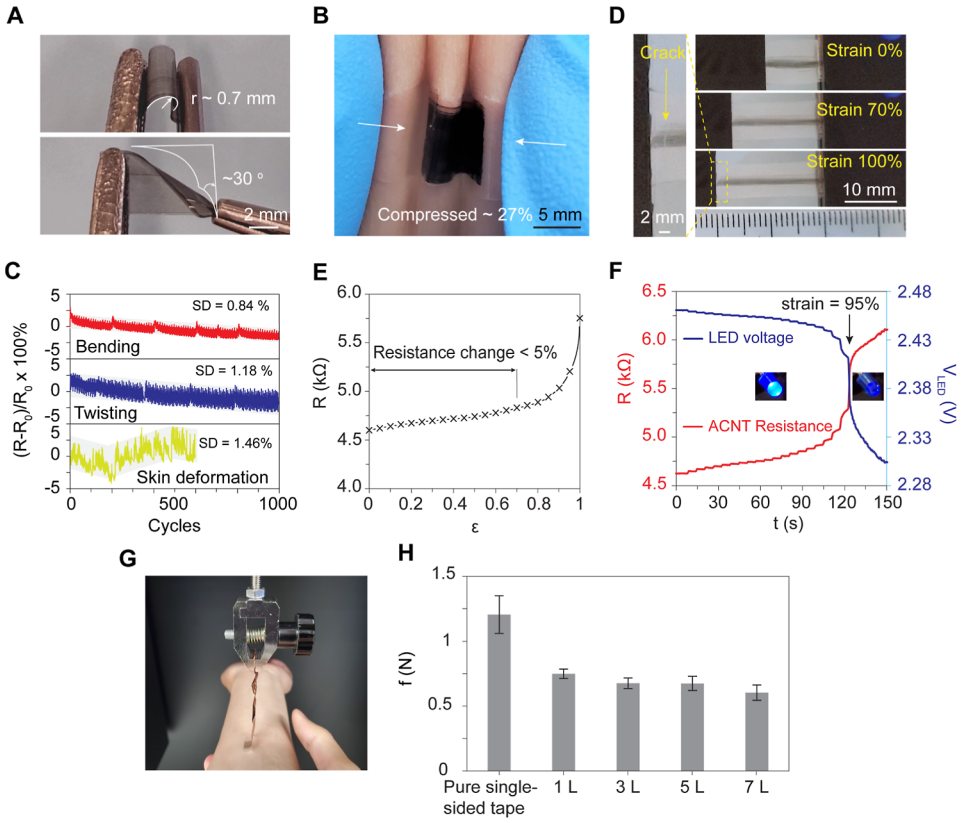

Figure 2. Electrical robustness of ACNT sheets under deformations and peeling of ACNT sheets on adhesive substrates from the skin. (A) Photos of an ACNT sheet under bending and twisting deformations. (B) Photo of an ACNT sheet on human skin under skin deformation. (C) Changes in the electrical resistance of a 7-layer ACNT sheet with respect to the number of deformation cycles; three types of deformations (twisting, bending, and skin deformation) are presented. R_0 is the initial electrical resistance, and R is the electrical resistance during deformations. SD is the standard deviation of electrical resistance changes. (D) Photos of the prestrained ACNT sheet at 0, 70, and 100% strain. The enlarged image represents a visible crack at 100% strain. (E) Strain dependence of the electrical resistance of the prestrained ACNT sheet. (F) Electrical resistance of the prestrained ACNT sheet and voltage of a blue LED with respect to time under strains, respectively. The left and right sections indicate the on and off states of the LED. (G) Measurement of peeling force by a 90° peel test. (H) Comparison of the peeling force between 1-layer, 3-layer, 5-layer, and 7-layer ACNT sheets on a single-sided tape and a pure single-sided tape. The error bars are standard deviations calculated from the corresponding peeling force signal in Figure S12.

sheets. The optical microscopy images of the sheets (Figure 1B) indicate their alignment, as well as their density (ACNT sheets with more layers look darker). Next, we applied a "tacky" transfer method by pressing an adhesive substrate onto the drawn ACNT sheets with the adhesive side facing the sheets, and the sample was then cut into portions. By peeling off the adhesive layers (the ACNT sheets were transferred and secured on the adhesive layers), we achieved the "tacky" on-skin electrodes that are thin, small, and flexible and can be directly attached to the human skin (Figures 1C and S1). Therefore, the overall process is facile and chemical-free and can be integrated into large-scale roll-to-roll manufacturing. It is worth mentioning that we used commercial adhesive tapes [made of poly(methyl methacrylate) (PMMA) or poly(vinyl alcohol) (PVA)] as adhesive substrates for a quick demonstration of proof-of-concept. In terms of nonadhesive substrates used for stacking ACNT membranes, they can be copper, aluminum, Teflon foil, or even the nonadhesive surface of a single-sided tape. However, a release liner is preferred because its easy release facilitates the detachment of ACNT sheets during transfer. However, the others could be stuck to adhesive substrates, resulting in difficulty in peeling off ACNT sheets and damage to the sheets (Figure S2).

The as-drawn ACNT sheets face a fragility problem that precludes them from direct contact with the skin (Figure 1D), whereas the transferred ACNT sheets show no visible damage against skin interaction or even during scratching by a pair of tweezers (Figure 1E,F and Movie S2). The transferred sheets are bonded securely to adhesive substrates due to the extrusion of adhesives through pores in CNT membranes.[24] The adhesives offer additional forces to hold CNTs firmly together apart from the van der Waals forces, reducing the separation and slippage between CNTs. This test indicates the excellent capability of ACNT sheets to be attached to human skin and act as on-skin electrodes without being physically damaged.

We characterized the electrical properties of the transferred ACNT sheets by measuring their electrical resistance, as shown in Figure 1G. Their resistance decreases as the number of stacked layers increases (increasing the thickness[30]). For example, a 1-layer ACNT sheet shows around 2 kΩ sq^{-1}, higher than around 200 Ω sq^{-1} for a 7-layer ACNT sheet due to the increase in the cross-section of the conduction path. Additionally, we investigated the morphology of a one-layer ACNT sheet by an atomic force microscope at three different positions (Figures 1H and S3), resulting in an average thickness of approximately 41 nm. Thus, its electrical

https://doi.org/10.1021/acsami.3c13541
ACS Appl. Mater. Interfaces 2023, 15, 58746−58760

conductivity was found to be around 1.2×10^4 S m^{-1}, which is in the range of the reported conductivities.[21]

The morphology shown in Figure S3 provides helpful information about the structure of ACNT sheets, which dictates their mechanical and electrical properties. First, CNTs were pulled out in parallel and formed bundles because of van der Waals forces. Second, junctions between CNTs and CNT bundles were also formed, as circled in those images. Third, as CNTs have not been twisted together like in yarn processing, CNTs or CNT bundles can still move/slip against each other. Based on that structure, as CNTs become more aligned (high degree of parallel), the number of junctions decreases, and their intertube contact enhances. These improvements allow for stronger interacting forces between the CNTs and the easier movement of electrons.[20,31] The results are higher conductivity and higher axial tensile strength, which can minimize the breakage of ACNT sheets.[21] In contrast, junctions and slippage negatively impact the electrical conductivity of the ACNT sheets. Junctions can form gaps that tend to enlarge gradually,[32] and slippage both increases the length of CNT bundles and reduces the intertube contact areas of CNTs;[31,33] hence, they hinder electron conduction. In brief, alignment enhances the electrical conductivity of ACNT sheets, while junctions and slippage have the opposite effect. Therefore, minimizing the occurrence of slippage and gap widening can effectively enable the electrical robustness of ACNT sheets against deformations, especially when the sheets undergo friction with the skin. We achieved robustness by transferring those sheets onto adhesive substrates by the facile "tacky" method.

2.2. Electrical Robustness of ACNT Sheets under Deformations. We investigated the electrical stability of a 7-layer ACNT sheet and a 3-layer ACNT sheet after transferring them onto flexible adhesive substrates (e.g., a conventional single-sided tape). They were subjected to bending deformations, twisting deformations, and skin deformations (Figures 2A,B and S4 and Movie S3). In the skin deformation test, the transferred sheets were attached to the skin and then compressed with the skin following the alignment direction of the sheets. The bending radius, twist angle, and degree of skin compression are approximately 0.7 mm, 30°, and 27%, respectively.

The experimental results show that bending and twisting deformations did not induce significant changes in the electrical resistance of the two sheets during 1000 cycles (less than 3%), as shown in Figures 2C and S5. These results are consistent with previous observations.[30,34] The portions of raw data of their resistance are given in Figure S6, showing small changes. A detailed explanation for this phenomenon is discussed in Note S1. Briefly, the calculated strains of CNTs are small, so they are unable to break them. Additionally, their length was roughly 400 μm (approximately the height of a CNT forest), long enough to maintain connections during bending.[31] Moreover, adhesive forces kept the CNTs/CNT bundles closed, minimizing the impact of slippage and gaps. However, the 7-layer sheet shows a greater change in electrical resistance than that of the 3-layer sheet. This can be the effect of slippage and gap widening in the outer layers of the 7-layer sheet because adhesives could not penetrate totally and uniformly to those layers compared to the 3-layer one (see illustration in Note S1). The drift behavior could be ascribed to two potential factors. The first is a result of the relaxation from polymer chains and the conductive network.[35] The second is the impact of the Joule-heating effect in the first few minutes after supplying voltage to the aligned CNTs, which show a negative temperature coefficient of resistance.[36] A detailed discussion is given in Note S2.

The effect of skin deformations on the electrical resistances was also minor, with resistance changes of less than 6% for the 7-layer and 3-layer sheets. However, the impact was stronger than that of bending and twisting deformations due to the influence of two possible additional factors. One is the friction between the sheets and the skin, which can distort the CNT structure. The other is the deformations that impair the contact between CNTs and the copper tape (used to connect ACNT sheets to the alligator clips of the measurement devices). The portions of raw data of their resistance are given in Figure S6.

We examined the electrical stability of a 5-layer ACNT sheet during stretching deformations. The sheet was transferred onto a stretchable substrate that was prestrained to 100% strain. The prestrained sheet exhibits a wrinkled structure, as illustrated in Figure S7. This structure can accommodate stretching deformations due to the buckling effect.[37] Since the human skin can be stretched to up to 70% strain,[12] we stretched the prestrained sheet to 100% strain for the electrical examination. The sheet was observed to be free of cracks within 70% strain, while a visible crack could be seen at 100% strain (Figure 2D). This observation was consistent with the measured electrical resistance of the sheet against strains (Figure 2E), where 70% strain corresponds to just a 5% resistance change. The negligible change in electrical resistance up to 70% strain, which can satisfy almost all the area in the human body,[7] is superior to the most common epidermal skin electrodes that show failure within 30% strain[10,13,15,26] or a large change in electrical resistance[12,27] during stretching.

We demonstrated the use of the prestrained 5-layer ACNT sheet by constructing a simple electronic circuit (Figure S8). The sheet acted as a stretchable resistor with an initial resistance of around 4.6 kΩ. It was connected in series to a group of conventional resistors that were parallel to a blue LED. Hence, we could observe the state of the LED to qualitatively evaluate the workability of the sheet during stretching deformations. The experimental results show that the LED remained bright until the sheet reached a strain of 95% (Figure S9 and Movie S4). For quantitative evaluation, we measured the LED voltage and the electrical resistance of the sheet in real time, as displayed in Figure 2F. During the strain up to 90%, the LED voltage decreased slightly, corresponding to a minor increase in the sheet's resistance. After that, the resistance surged because of the crack shown in Figure 2D, resulting in a steep drop in the voltage. This measurement is consistent with the above observation, confirming the electrical stability of the prestrained ACNT stretchable resistor.

For a comprehensive study, we also examined the electrical stability of a nonprestrained ACNT sheet. Another 5-layer ACNT sheet was transferred onto the same type of stretchable substrate, but the substrate was not prestrained. The nonprestrained sheet was also integrated into the same electronic circuit with an initial resistance of roughly 2.6 kΩ. We quickly observed the off state of the LED after stretching the sheet to 15% (Figure S10 and Movie S4). The electrical resistance of the sheet and the LED voltage were also measured, showing a dramatic increase in resistance and a sudden decrease in the voltage after 15% strain. This poor performance of the sheet is due to the early appearance of

https://doi.org/10.1021/acsami.3c13541
ACS Appl. Mater. Interfaces 2023, 15, 58746−58760

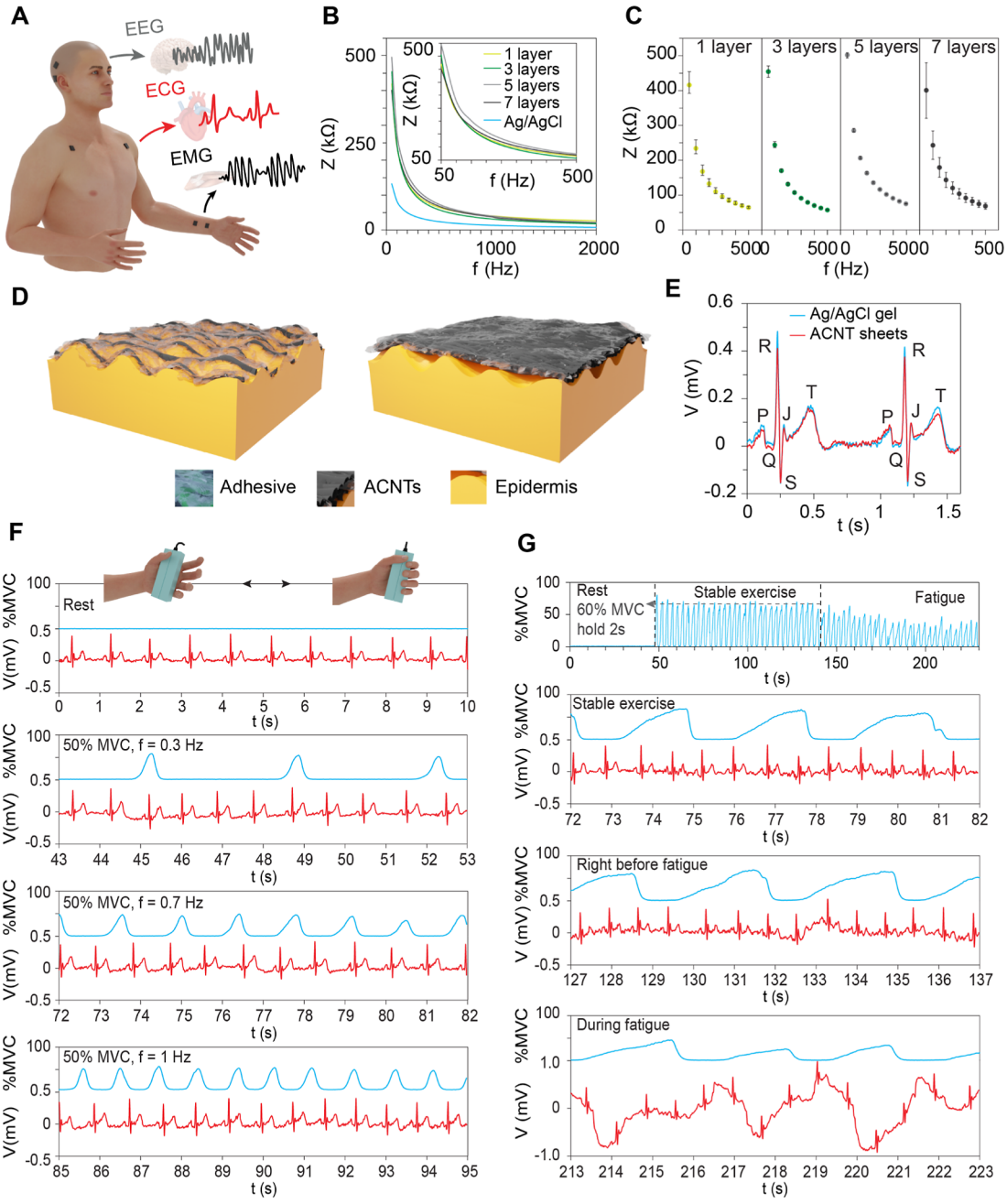

Figure 3. Measurement of contact impedance and monitoring of ECG signals under hand grip exercise. (A) Illustrative image of the placement of electrode pairs for monitoring human electrophysiological signals (black pads represent ACNT sheets). (B) Comparison of contact impedance between ACNT sheets with different layers and commercial Ag/AgCl gel electrodes. The frequency ranges from 50 to 2000 Hz. Inset: an enlarged image showing the clear difference in contact impedance measured from ACNT sheets. (C) Comparison of errors of contact impedance measured from ACNT sheets with different layers. The mean values are determined by measuring the impedance three times, and the maximum and minimum values are presented as error bars. (D) (left) Illustration of the infiltration of adhesives into pores in sparse ACNT bundles, bringing the bundles close to the skin. (right) Illustration of dense ACNT bundles that hinder the infiltration of adhesives, resulting in nonconformal contact with the skin. (E) ECG signals recorded by ACNT sheets and commercial electrodes, with crucial waves (P wave, QRS complex, T wave, and J point) presented. (F) Stability of ECG signals measured from ACNT sheets at rest and under low artifacts from a hand grip exercise with 50% of the participant's maximum voluntary contraction (MVC) at different frequencies. (G) Effect of intense artifacts on ECG signals from a hand grip exercise maintained at 60% MVC with repeated 2 s hand contractions alternated with 2 s of relaxation until fatigue.

cracks at 15% strain (Figure S10). It is worth mentioning that its initial electrical resistance (2.6 kΩ) was almost half the value of the prestrained one (4.6 kΩ); hence, the resistance is further from the critical value for switching the LED off. However, the nonprestrained sheet rendered the LED off faster than its counterpart, indicating the superior performance of the latter.

To examine the effect of prestretching an ACNT sheet in another direction (prestrained to 100%), we have prestrained and then stretched an ACNT sheet in the transverse direction (perpendicular to the alignment direction) (Figure S11). The sheet can retain its electrical resistance (<5% changes) up to a strain of 26%, higher than that of the corresponding nonprestrained one as expected (6% strain). So, our transfer

https://doi.org/10.1021/acsami.3c13541
ACS Appl. Mater. Interfaces 2023, 15, 58746−58760

method offers a simple approach for generating a stretchable resistor and a stretchable electrode for electronic skin[38] or a stretchable bridge for circuit connection.[39]

As the ACNT sheets should be attached on the skin for electrophysiological monitoring, we measured the peeling force of ACNT sheets on a single-sided tape by the 90°-peeling test[40] (Figures 2G and S12). Although the deposition of ACNT sheets on the tape reduces the adhesive force of the tape, the peeling force of 3-layer and 5-layer ACNT sheets on the tape is around 0.67 N (0.39 N cm^{-1}), the highest is about 0.75 N (0.44 N cm^{-1}) for the 1-layer ACNT sheet (Figure 2H), and the 7-layer ACNT sheet has the lowest peeling force (about 0.6 or 0.35 N cm^{-1}). This is because the one-layer ACNT sheet has a low density of CNTs (Figure 1B), allowing more adhesives to penetrate through pores and reach the skin. However, the 7-layer ACNT sheet has a high density of CNTs, blocking the penetration of adhesives. The results of the peeling force are consistent with the observation of the change in the electrical resistance of ACNT sheets under deformations (Figures 2C and S5). The peeling force of the 3-layer sheets after 3 h is given in Figure S13, showing an overall decrease in the force owing to skin wetting. We also measured the peeling force of an ACNT sheet on a viscous stretchable tape (Figure S14). The sheet on the tape has a higher peeling force than the sheet on the single-sided tape due to the higher adhesion of the pure viscous tape compared to the single-sided tape. However, the viscous tape is too thick (~1000 μm thickness), which is not appropriate for skin-worn devices. Then we use the conventional ACNT sheets on a single-sided tape as epidermal sensors (the thickness of the tape is ~60 μm). It is worth mentioning that future optimization on adhesion and thickness of substrates is desired as the ACNT sheets can be easily deposited on different types of substrates.

2.3. ACNT Sheets as On-Skin Sensors. ACNT sheets exhibited a sturdy structure and electrical robustness upon skin contact and skin deformation after being transferred onto adhesive substrates. As a result, we utilized those transferred sheets as "tacky" epidermal sensors to monitor the human electrophysiological signals. ACNT sheets act as measuring electrodes and are in direct contact with the skin. We chose the electrode size of 8 mm × 8 mm as it has been reported that the dimension of the electrode should be less than 10 mm for optimal results.[9,41] We placed the sheets in different positions to obtain the ECG, EMG, and EEG signals (Figure 3A). These signals were also recorded via commercial Ag/AgCl gel electrodes to validate the performance of the ACNT sheets. However, as the signal quality is highly dictated by sensor−skin interface impedance,[42] we measured the contact impedance of an ACNT sheet−skin interface and a gel electrode−skin interface beforehand. The measurement was taken without skin preparation in the frequency range of 50−2000 Hz when the sheets and the gel electrodes were positioned on the left forearm of a human subject (Figure S15A).

The contact impedance between the skin and ACNT sheets with different layers is quite similar. However, 1-layer, 3-layer, and 7-layer ACNT sheets show lower contact impedance than the 5-layer ones (Figure 3B,C). Higher conductivity[43] and higher density (higher contact area)[44] are expected to lower the contact impedance. Thus, the low impedance of 7-layer ACNT sheets is understandable as they have the highest conductivity (Figure 1G) and high density (Figure 1B). However, 1-layer and 3-layer ACNT sheets also show lower contact impedance because of the assistance of adhesives. Due to the fact that those sheets contain sparse ACNT bundles compared to 5-layer and 7-layer ACNT sheets, adhesives can penetrate through pores more and provide additional adhesive forces to make 1-layer and 3-layer ACNT sheets close to the skin. This benefits more contact areas, minimization of gaps, and a secure interface between ACNT bundles and the skin (Figure 3D, left panel). Nevertheless, the one-layer ACNT sheets show a large bias in their sheet resistance (Figure 1G), which affects the stability of their contact impedance (large errors shown in Figure 3C). Similarly, the large errors of contact impedance are also observed in the case of the 7-layer ACNT sheets (Figure 3C). Although the 7-layer sheets have a small bias in the sheet resistance, the dense ACNT bundles hinder the penetration of adhesives, reducing the benefit of adhesive forces to bring the bundles close to the skin and tightening the existing contact between the bundles and the skin (Figure 3D, right panel). In contrast, the 3-layer and 5-layer ACNT sheets exhibit stable contact impedances (Figure 3C) due to their high conductivity, small bias in their conductivity (sheet resistance), and moderate density of ACNT bundles that allow the additional adhesive forces to provide conformal contact with the skin. The effect of sweat on the contact impedance is shown in Figure S16. The impedance of the 3-layer sheets decreased after 3 h, which is consistent with previous reports.[45] We have also measured the contact impedance of one-layer ACNT sheets on viscous stretchable substrates as shown in Figure S17. Their impedance is lower than that of 1-layer ACNT sheets on flexible single-sided tapes and higher than that of commercial electrodes. This can be attributed to the higher adhesive force of the viscous substrates as mentioned above (Figure S14), leading to minimizing air gaps between the skin and the devices. Therefore, ACNT sheets on viscous substrates can be good epidermal sensors. However, the aforementioned 1000 μm thickness makes the sensors bulky and should be optimized in future work because thinner substrates also help minimize gaps at the skin−device interface and improve signal quality.[9] When compared to the device−skin electrical impedance of the commercial Ag/AgCl gel electrodes, ACNT sheets on flexible single-sided tapes exhibit higher impedance values as shown in Figure 3B. This can be ascribed to the smaller working area of the ACNT sheets (64 mm^2) compared to that of the commercial ones (401 mm^2)[9,44] and less conformal contact with the skin. The effect of area on the impedance was confirmed by the measured contact impedance of 121 mm^2 and the original (401 mm^2) commercial electrodes given in Figure S18. The less conformal contact with the skin was previously analyzed with ACNT sheets on viscous substrates (Figure S17). Therefore, there is still room for improvement. However, to demonstrate the capability of using ACNT sheets for effective monitoring of electrophysiological properties, we utilized either 3-layer or 5-layer ACNT sheets on flexible single-sided tapes in the following measurement.

As shown in Figure 3E, we achieved the ECG signals of both ACNT sheets and commercial electrodes by placing those in the left and right subclavicular spaces while the reference electrode (Ag/AgCl gel) was on the right iliac crest[46] (Figure S15B). The signals were filtered through a biobandpass filter between 0.3 and 50 Hz. The ECG signals obtained from ACNT sheets are comparable to those from commercial electrodes, showing explicitly the crucial waves (P wave, QRS complex, T wave, and J point). The magnitude of the R peak of ECG from the ACNT sheet is smaller than that from

https://doi.org/10.1021/acsami.3c13541
ACS Appl. Mater. Interfaces 2023, 15, 58746−58760

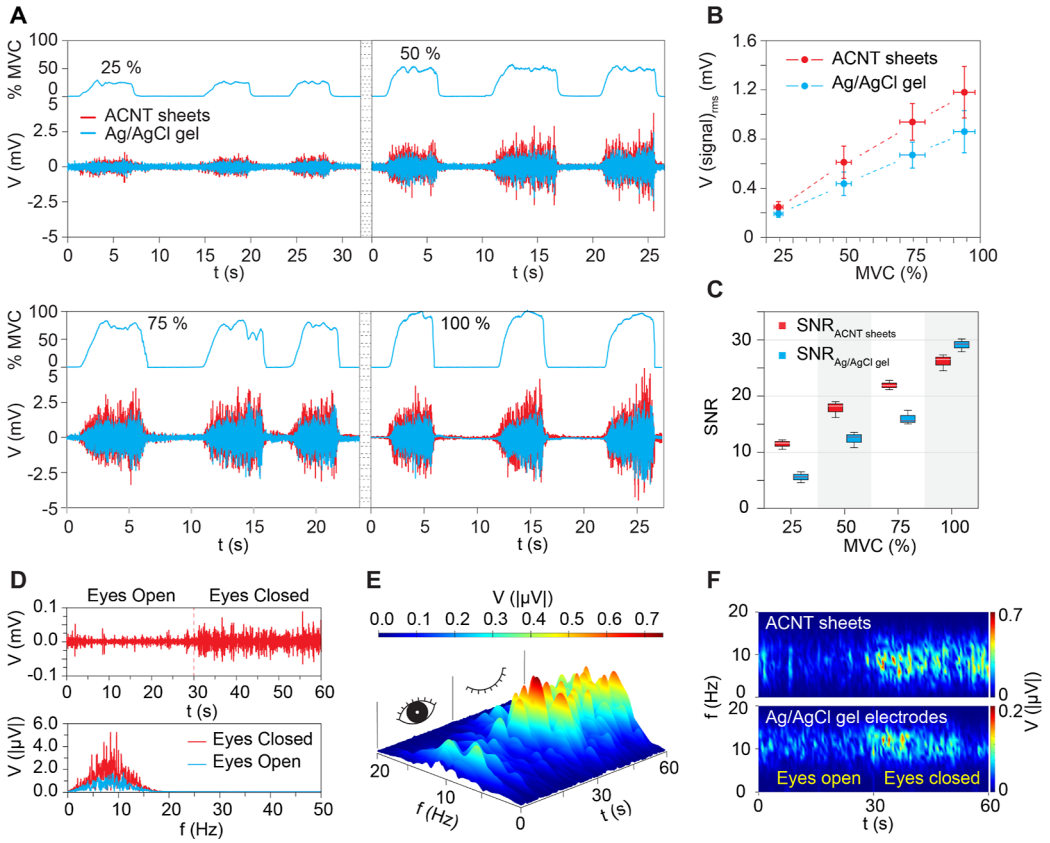

Figure 4. Monitoring of EMG and EEG signals. (A) EMG signals measured by ACNT sheets and commercial electrodes at designated grip forces of 25, 50, 75, and 100% MVC. (B) Linear relationship between the mean values of the root-mean-square of the EMG signals and the magnitude of MVC. Error bars represent standard deviations calculated from the root-mean-square values. (C) Comparison of SNRs of EMG signals obtained by ACNT sheets and commercial electrodes at different MVCs. (D) EEG signals recorded by ACNT sheets with the signal in the (top) time domain and (bottom) frequency domain. (E) 3-D view of a time-frequency spectrogram of the EEG signals recorded by ACNT sheets. (F) 2-D view of the time-frequency spectrograms of EEG signals recorded by ACNT sheets (top) and commercial electrodes (bottom).

commercial electrodes because of the higher contact impedance shown in Figure 3B. However, the Pearson's coefficient, r, between the two signals is calculated by

$$r = \frac{n(\sum xy) - (\sum x)(\sum y)}{\sqrt{[n\sum x^2 - (\sum x)^2][n\sum y^2 - (\sum y)^2]}}$$

Here, n is the number of elements in the data. x or y is the element of the ECG data from ACNT sheets and commercial electrodes. Thus, r is calculated to be ~0.98, showing excellent similarity of the ECG signals decoded by the sheets and the commercial electrodes. Besides, the signal-to-noise ratio (SNR) of ECG using ACNT sheets is 21.22 ± 0.74 dB, similar to that of commercial ones (21.57 ± 0.57 dB). It also confirms that the performance of ACNT sheets is comparable to that of commercial electrodes. The stability of ECG signals from the sheets is shown in the top image in Figure 3F (at rest), proving the workability of the ACNT sheets in achieving continuously reliable heart signals. The above ECG signals were obtained by the 5-layer ACNT sheets and commercial electrodes. In comparison, the 3-layer sheets also show similar performance to the commercial electrodes and lower R peaks. Detailed information and discussion are given in Figure S19.

Then, we examined the influence of artifacts from a hand grip on the quality of the ECG signals. The participant was asked to hold a grip dynamometer tightly by the dominant hand to assess the MVC. The MVC was estimated by taking a maximum of three holding attempts. With the interference of the low artifacts from the hand grip exercise (i.e., 50% MVC at different frequencies), the ACNT sheets still exhibit excellent stability (Figure 3F). Accordingly, the increase in heart rate (HR) can be clearly observed due to the denser R peaks (typically, from ~62 to ~78 bpm). However, the intense exercise can induce larger artifacts to the ECG signals (Figure 3G). The participant was asked to maintain a MVC of 60% with repeated 2 s hand contractions alternated with 2 s of relaxation until fatigue. When the participant can maintain the grip force during the exercise, the ECG signals exhibit stable performance with minimal effects from artifacts. But right before fatigue happened, the artifacts elevated the signal, and during the fatigue, the ECG signals were distorted following the frequency of the applied grip force. This distortion can be ascribed to the possibility that the muscle in the forearm of the participant cannot be maintained during the fatigue stage. Therefore, the participant must use muscles from the shoulder (by forcefully shrugging the shoulder) to maintain the designated % MVC during 2 s, which can displace the sheets a little (the sheets are positioned near the shoulders). However, the HR during the intense exercise can still be deduced and shown in Figure S20, with the increase in HR from ~62 bpm at rest to ~85 bpm during the exercise and fatigue stages, which is compatible with previous findings.[47] The increase in HR is attributed to the increase in oxygen consumption.[48] It is worth noting that minimizing the effect of

https://doi.org/10.1021/acsami.3c13541
ACS Appl. Mater. Interfaces 2023, 15, 58746−58760

intense artifacts can be done by improving the stability of the sheet−skin interface. As the sheets are already nanoscale in thickness, the minimization can be achieved by making the adhesive substrate thinner, softer, or stickier.[49]

Using the same grip dynamometer and the same MVC scale, we compared the EMG signals measured from the ACNT sheets and commercial electrodes. They were placed alternately on the right forearm and near the wrist (Figure S15C). A reference electrode was attached at the elbow of the same arm. As the EMG signals reflect the muscle contractions in the forearm, which are triggered by hand squeezing,[50] the participant was asked to maintain different levels of designated grip force (MVC of 25, 50, 75, and 100%). We obtained the EMG signals corresponding to each MVC after filtering them through a biobandpass filter (1−500 Hz). As shown in Figure 4A, the sheets captured higher EMG signal magnitudes compared to the commercial electrodes. In addition, raising the MVC triggered larger EMG signal responses, as confirmed by calculating the signals' root-mean-square (rms) (Figure S21). Hence, we achieved a linear relationship between the rms values and the MVC (Figure 4B), with the angular constant for the commercial electrodes (0.96 mV) being smaller than that for the sheets (1.34 mV). This can be attributed to the different positions of the sheets and the commercial electrodes on the forearm. The commercial electrodes were placed nearer to the tendon area. This area has fewer and thinner muscle fibers, thus triggering less EMG signals.[51] Therefore, the corresponding SNRs of EMG signals obtained by ACNT sheets are comparable to or even higher than those of commercial electrodes (Figure 4C). It can also be seen that raising the MVC increases the SNRs as the amplitude of signals increases accordingly.

We recorded EEG signals by placing ACNT sheets and commercial electrodes on the left and right posterior lobes behind the ears. The reference electrode was placed on the right mastoid bone (Figure S15D). During the EEG test, the participant was instructed to maintain open eyes for 30 s and then close the eyes for 30 s. Since the eyes-closed state is known to elicit alpha waves in the brain (frequency range of 8−12 Hz),[52] the EEG signals were filtered through a biobandpass filter (1−60 Hz), followed by a digital bandpass filter (8−12 Hz). Then, the EEG signal recorded by the sheets was analyzed and displayed in the time domain and frequency domain, showing the two distinct states of the eyes (Figure 4D). Also, the frequency peaks concentrate around 9 Hz in the eyes-closed state, consistent with prior studies.[53] A short time Fourier transform (STFT) was applied to attain the time-frequency spectrogram of the signal, revealing the consistent presence of alpha waves throughout the eyes-closed state (Figure 4E). Regarding EEG signals recorded by commercial electrodes (Figure S22), the signal analysis indicates inferior performance, as the time domain and frequency domain did not show a clear difference between the two states of eyes. Moreover, the time-frequency spectrogram exhibits inconsistent activity at the end of the eyes-closed state (Figure 4F). The sheets and the commercial electrodes differ in EEG monitoring performance because of their positions[53] and the negative impact of hair on contact impedance.[54] We performed a compatibility test by continuously wearing ACNT sheets on the arm of a participant for 24 h. The skin under ACNT electrodes did not show any evidence of itching or erythema during and after the test (Figure S23). However, more study (such as growing cells on ACNT sheets on substrates) is necessary. The comparison in measuring electrophysiological signals between ACNT sheets and other materials in previous work is given in Table S1. The monitoring performance of ACNT sheets is comparable to that of other sensors made from silver flakes, silver nanowires, or conductive polymers. However, enhancing adhesion in future work could improve the stability of the ACNT epidermal sensors. Besides, ACNT sheets show high performance in decoding those signals compared to that of random CNTs. ACNT sheet-based electrodes possess excellent stability and good adhesion force owing to their alignment and porous structure. It is noteworthy that the alignment offers CNTs unique advantages over the nonaligned ones in terms of high electrical conductivity[21] achieved for an ultrathin nanomembrane structure, resulting in a low density of CNTs for electronic applications that require high conductivity. These distinct properties have recently attracted considerable interest.[23,55]

In comparison to the state-of-the-art digital printing technologies such as inkjet printing,[56] aerosol jet printing,[57] or direct ink writing,[58] our simple stamping method using aligned CNT sheets for health monitoring is in an early stage of development. Then, work is still needed to identify the limitations of the method to improve and expand its capabilities. However, highlighting the strengths and limitations of each approach is necessary. Those printing techniques benefit a variety of materials for ink and substrates, customization of electrode shapes, integration of complex circuits, high resolution, fast printing, and the capability to be integrated in roll-to-roll mass production. However, the ink formation and formula are not straightforward to ensure meeting rheological criteria such as ink viscosity, surface tension, shear-thinning, and yield-stress. Besides, the need for postprocessing (optimal sintering temperature and time) is indispensable to ensure the electrical and mechanical reliability of devices, which can overall complicate the production process (such as the integration of additional pulse thermal processing techniques). On the other hand, our stamping method with aligned CNT sheets also offers quick fabrication of electrodes and conductive paths, the capability to be integrated in roll-to-roll mass production, and a solution-free process. It does not need to meet those strict criteria for ink preparation and may not require a postprocessing process. Nevertheless, there are also parameters needed to optimize the uniform growth of CNTs using chemical vapor deposition such as reaction temperature and gas flow rate. Besides, the first pulling to get a uniform ACNT membrane could be challenging, and it is not easy to make customized shapes using ACNT sheets. The substrates should be adhesive to transfer and hold the sheets securely. The additional process of prestretching substrates may be needed to ensure stable electrical properties under deformation, which could hinder their integration in automatic mass production.

2.4. Sustainable ACNT Sheets on Soluble Substrates.

In order to promote the sustainable production of CNT-based devices, we transferred ACNT sheets onto PVA substrates, referred to as PACNT sheets. The PACNT sheets can function as epidermal sensors, working the same as the aforementioned ACNT sheets on flexible substrates (conventional single-sided tape). However, unlike the flexible tape that is hard to dissolve, PVA features a biodegradable property and quick dissolution in water,[59] favoring its application in sustainable health monitoring.[60] Hence, PVA substrates can be dissolved to

https://doi.org/10.1021/acsami.3c13541
ACS Appl. Mater. Interfaces 2023, 15, 58746−58760

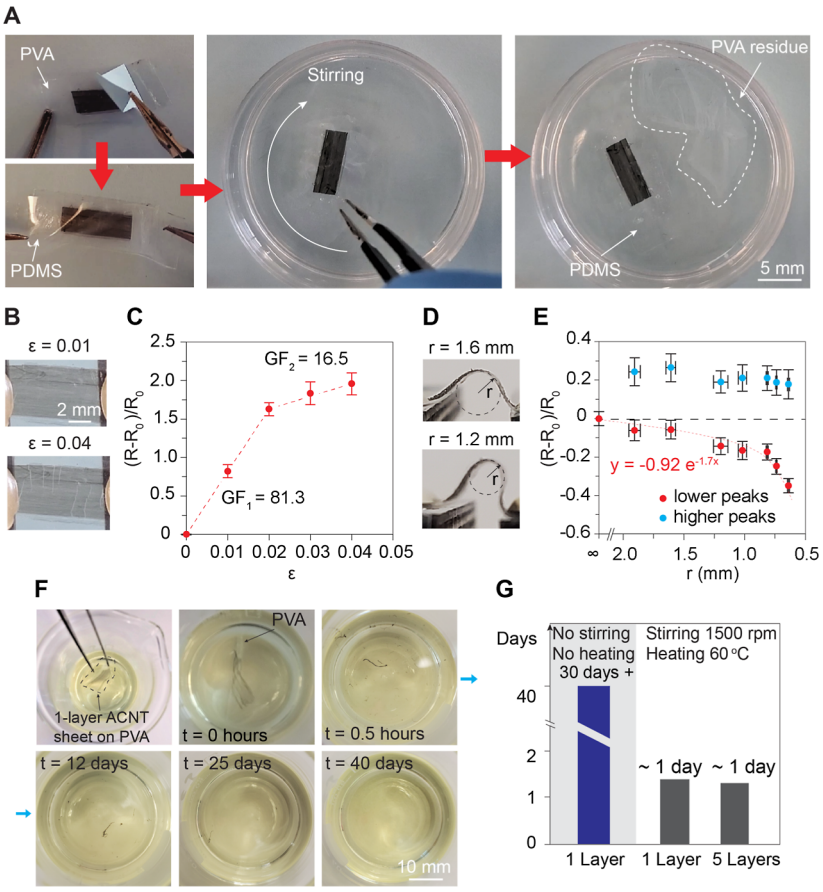

Figure 5. Reusability and degradability of an ACNT sheet on a soluble adhesive substrate. (A) Photos of the process of reusing a 5-layer ACNT sheet, including (top left) transferring the sheet onto a PVA substrate using our facile transfer method (referred to as PACNT sheet), (bottom left) pressing a PDMS (facing CNTs) on the PACNT sheet, (middle) immersing the PACNT sheet (attached to the PDMS) in water and stirring the water to facilitate PVA detachment, and (right) the detachment of the PVA, leaving CNTs on the PDMS substrate. (B) Photos of invisible cracks and visible cracks in the reused sheet at 0.01 strain and 0.04 strain, respectively. (C) Changes in electrical resistance vs strains of the reused sheet. (D) Photos of bending curves with the radii of 1.6 and 1.2 mm. (E) Changes in electrical resistance vs bending radii of the reused sheet (blue dots indicate that the reused sheet returned to its original position, and red dots indicate that the reused sheet reached the end of the bending process). Error bars in parts (C,E) represent the standard deviation calculated from the peak values of the corresponding real-time data. R_0 is the initial electrical resistance, and R is the electrical resistance during deformations. (F) Photos of the degradation process of a 1-layer PACNT sheet. (G) Bar chart showing the comparison of degradation time between a 1-layer PACNT sheet without external factors (stirring and heat) and 1-layer and 5-layer PACNT sheets with external factors.

facilitate the reuse or degradation of PACNT-based electronic devices (Figure S1C).

We demonstrate the reusable capability of a PACNT sheet by shifting the ACNT sheet from the PVA substrate to a PDMS substrate; the ACNT sheet on PDMS then becomes a strain sensor. The shifting process is illustrated in Figure 5A and Movie S5, in which one-layer and five-layer ACNT sheets were used to demonstrate the capability to transfer multilayer sheets. First, a thin layer of PDMS was deposited on a PACNT sheet with the PDMS in contact with the ACNT surface. Then, the sample was immersed in water, followed by stirring the water to facilitate PVA detachment. Once the PVA was detached, the ACNT sheet remained adhered to the PDMS due to the adhesion between them, referred to as an ACNT-PDMS sheet. Finally, the ACNT-PDMS sheet was taken out of the water and dried in the air for one day. The photos of the 5-layer ACNT sheet on either PVA or PDMS (Figure S24) indicate that the sheet structure was preserved during the shifting process, although some CNT bundles could be lost during the PVA detachment procedure. The electrical resistance of the dried sheet was initially around 5.6 kΩ (3 kΩ sq^{-1}). However, it increased to about 20 kΩ after being loaded on a testing machine. The increase in resistance is ascribed to the appearance of cracks (Figures 5B and S26A), which implies the fragility of the ACNT sheet on the PDMS. This further affirms the efficiency of using adhesive forces to reinforce the ACNT sheets.

Regardless of the resistance increase, the ACNT-PDMS sheet can function as a strain sensor based on the crack effect.[61] We stretched the sheet and measured its change in resistance, as shown in Figure S25A. The cracks can be clearly seen in Figure 5B at 4% strain and in Figure S26A. The resistance responded linearly to strains in two regions (Figure 5C). One is up to 2% strain, and the other is from 2% strain to 4% strain. The gauge factor is defined as GF = $(\Delta R/R_0)/\varepsilon$, in which R_0 is the initial electrical resistance, ΔR is the change of electrical resistance with respect to the initial resistance, and ε is the strain. Hence, the gauge factors are calculated as GF_1 = 81.3 in the first region and GF_2 = 16.5 in the second region. Besides stretching deformations, we also bent the sheet and obtained its resistance in response to the bending radii (Figure 5D). The real-time data are given in Figure S25B. The data

https://doi.org/10.1021/acsami.3c13541
ACS Appl. Mater. Interfaces 2023, 15, 58746−58760

includes high and low peaks. The high peaks imply that the sheet returned to its original position. At that point, it was stretched a little due to a quick change in direction, leading to an increase in its electrical resistance. In contrast, the low peaks indicate that the sheet has reached the end of the bending process. Bending the sheet could help narrow the crack gaps of the sheet, reducing the distance between CNTs on the two sides of the gaps (Figure S26B,C). As a result, the sheet's electrical resistance decreases upon bending deformations. Thus, we use the low peaks to evaluate how the sheet's electrical resistance depends on the bending radii. The calculation indicates an exponential relationship between them, as depicted by the fitting curve $y = -0.92\ e^{-1.7x}$ (x represents the bending radius and y represents a change in electrical resistance) (Figure 5E). This exponential behavior can be explained by Simmons's theory for tunneling resistance that exponentially depends on the tunneling distance between adjacent CNTs.[62] The visualization of the bending process is provided in Figure S26B. These tests demonstrated the reusability of the ACNT sheet. It is worth mentioning that the reused sheet was not postprocessed before the tests; hence, its performance could be improved by further treatments, such as using ethanol or alcohol to densify CNTs.[34,63] Then, the reused ACNT sheets can also act as active elements in respiration sensors, for example.[64]

When it comes to the degradability of PACNT sheets, a PVA substrate can be quickly dissolved in a water solution. However, CNTs are tricky to degrade because of their strong physical and chemical stability; hence, their degradation requires the presence of microbes, enzymes, or macrophages.[65] In this test, we utilized sodium hypochlorite (NaClO) solution to degrade PACNT sheets as it was proven to degrade CNT waste owing to the oxidizing ability of ClO^- that is also created from enzymatic reactions.[66,67] Figure 5F displays the degradation process of a 1-layer ACNT sheet on a PVA substrate (a 1-layer PACNT sheet). We placed it in a liquid chlorine solution (common bleach containing 13% NaClO) and then stirred it for a few minutes to break down the ACNT sheet and the PVA substrate. Then, the sample was left intact at room temperature (about 25 °C). The PVA disappeared after 30 min, but CNTs took weeks to degrade. During the degradation process, it was observed that thinner and shorter CNT aggregates degraded faster than thick and long ones. This was due to NaClO molecules colliding with the outer CNTs before reaching the inner CNTs of the aggregates. The collisions evoked chemical reactions, $C_{CNT} + 2NaClO \rightarrow CO_2 + 2NaCl$, where CO_2 could be transformed to carbonate ($[CO_3^{2-}]$ or $[HCO_3^-]$). Thus, CNTs were degraded into oxidized graphene sheets as intermediate products, which were further degraded into carbonate and carbon dioxide as the final products of the degradation process.[67]

We conducted another degradation test with 1-layer and 5-layer PACNT sheets to assess the effect of external factors (stirring and temperature) (Figure S27). They were also placed into the same liquid chlorine solution but subjected to stirring and high temperatures (1500 rpm and about 60 °C, respectively). However, there were no external factors overnight (almost 18 h). Their degradation rates were observed to be much faster than the previous 1-layer sheet (around 1 day compared to weeks) (Figure 5G). Note that the sizes of these two sheets were smaller than the previous one, but CNT aggregates were observed in all cases. Such aggregates were the main problem of degrading CNTs, as seen in the case of the previous sheet. Hence, the results of the faster degradation rates indicated that stirring assisted in separating thick aggregates due to the friction between themselves and between them and the solution. In addition, the high temperature increased the molecules' dynamics, leading to an increased collision frequency between CNTs and NaClO molecules. We have not found any evidence of the disposability of ACNTs in the sweat environment. In addition, the choice of substrate will affect the disposable capability of the electrodes. For example, if CNTs are integrated in PDMS, other chemicals than NaClO must be utilized to degrade the electrode.[68]

Regarding economic viability, the estimated cost of a 3-layer ACNT sensor can be as low as ~0.2 USD. The price can be significantly dropped when CNT forests are mass-produced. The cost of ACNT sensors can be reduced further as they are reusable.

3. CONCLUSIONS

We have presented a facile method using a "tacky" surface to create a tight sensor−skin interface for skin-worn electronics made of ACNT sheets. The electrodes are free of damage upon skin contact and are electrically robust during deformations. High stretchability up to 70% strain enables ACNT electronics to serve all applications related to contact with human skin. The "tacky" sensing surface with a moderate density of ACNT bundles provides a tight interface between the device and the skin, enabling the capture of high-quality ECG, EMG, and EEG signals with the minimization of impact from motion artifacts. The demonstrations of reusing ACNT sheets as a strain sensor and degrading the sheet-based electronics provide a comprehensive use of ACNT sheets as on-skin electronics and foster the use of sustainable devices. However, with further optimization on the substrates (thinner and more breathable), the ACNT sheet-based electronics can work more reliably on the skin without causing suffocation. Further efforts should be put into producing the curvature of ACNT sheets/ribbons to upscale their functions as electronics.

4. EXPERIMENTAL SECTION

4.1. Fabrication of ACNT Sheets via Dry Spinning. A razor blade was used to draw an ACNT membrane from a CNT forest growing on a silicon wafer via a chemical vapor deposition (CVD) process. The membrane was slowly pulled out, forming a continuously long ACNT membrane. The pulled CNT membrane was then deposited gently on the nonadhesive substrate that was wrapped around the side of a drum-like pulley. The nonadhesive substrate could be aluminum, copper foil, the nonadhesive side of a single-sided tape, or the release liner of a copper tape. Afterward, the pulley was spun at a speed of 5° s^{-1}. Each rotation of the pulley yields one layer of an ACNT sheet. Therefore, one-, three-, five-, and seven-layer ACNT sheets correspond to 1, 3, 5, and 7 turns of the pulley (Movie S1). Then, the ACNT sheets on the nonadhesive substrates were released from the pulley and stored for later use. Since the ACNT sheets are easily shattered and broken, they should not touch other objects during storage.

4.2. Transfer ACNT Sheets onto Flexible Adhesive Substrates. A layer of single-sided tapes (crystal clear tapes, staples) was deposited on one of the ACNT sheets that were previously drawn on nonadhesive substrates. The adhesive side of the tape was in contact with the ACNT sheet. The tape was pressed with a small force to ensure a complete transfer of the ACNT sheet to the tape. Then, the nonadhesive substrates were peeled off, leaving the ACNT sheet mounted on the tape. The ACNT sheets on the tape were cut into different portions (8 mm × 8 mm working area) to measure their

https://doi.org/10.1021/acsami.3c13541
ACS Appl. Mater. Interfaces 2023, 15, 58746−58760

electrical resistances. They were also placed on human skin to monitor human biopotential signals (Figure S1A).

4.3. Transfer ACNT Sheets onto Stretchable Adhesive Substrates. A 5-layer ACNT sheet on a nonadhesive substrate was carefully cut into two narrow sheets, 1 cm long and 2 cm long. A stretchable tape (3 M VHB double-sided tape, Scotch brand) was cut into two 2 cm-long pieces. One piece was stretched to twice its original length (i.e., its length became 4 cm) and kept that way. Then, the 2 cm-long ACNT sheet was transferred onto it by the same transfer method as that used by the single-sided tape. After peeling off the nonadhesive substrate, the stretched piece was released to its original length. Consequently, the 2 cm-long ACNT sheet shrank to 1 cm due to the contraction of the stretched piece (Figure S1B). Then it was defined as a prestrained ACNT sheet. The other 1 cm-long ACNT sheet was also transferred onto the remaining stretchable piece that was not initially prestrained. This one was defined as a nonprestrained ACNT sheet. The prestrained and nonprestrained ACNT sheets in the transverse direction (perpendicular to the alignment direction) are obtained in the same ways, and the 3-layer ACNT sheets were used.

4.4. Transfer ACNT Sheets to Soluble Adhesive Substrates. 1-layer ACNT sheets and 5-layer CNT sheets were transferred to PVA adhesive tape (water-soluble wave solder tape 5414, 3 M) by the same transfer method as using single-side tapes (Figure S1C).

4.5. Electrical Characterization of ACNT Sheets under Bending, Twisting, and Skin Deformations. Copper tape was attached at the two ends of an ACNT sheet on a flexible substrate to make a connection to the measurement devices. The sheet's electrical resistance was measured by a hand-held LCR meter 879B or recorded in real time via a Keithley source meter 2450 connected to Kickstart software. A 3-layer and a 7-layer ACNT sheet a on single-sided tape were loaded on a home-built linear motor and connected to the measurement devices (Keithley source meter 2450). Their electrical resistance was measured, while they were bent and twisted with a bending radius of approximately 0.7 mm and a twist angle of 30°. The tests were conducted for 1000 cycles for each type of deformation. Then the two sheets were placed on the upper part of the participant's left forearm. They were compressed and released with the skin for 500 or 600 cycles, while their electrical resistance was also measured by the Keithley source meter 2450.

4.6. Electrical Characterization of ACNT Sheets under Stretching Deformations. A copper tap was also used to make a connection to the measurement devices. The prestrained or nonprestrained ACNT sheet on stretchable substrates was connected in series to a group of resistors (almost 8.3 kΩ) that was paralleled to a blue LED (Figure S8). A supply voltage of 4 V was applied to the circuit. The two sheets were loaded on the same linear motor and stretched to 100% strain, while their voltage was measured via the Keithley source meter 2450. The visualization of the tests is given in Movie S4. Their electrical resistance was derived from the measured voltage and the UI curve of the LED (Figure S28) following the below formula

$$R_{CNT} = \frac{V_{CNT}}{\frac{V - V_{CNT}}{R_0} + I_{LED}}$$

Here, R_{CNT} is the electrical resistance of a stretchable resistor under strain. V is the supply voltage (4 V); V_{CNT} is the measured voltage of the ACNT sheets. R_0 is the resistance of the group of resistors (8.3 kΩ). I_{LED} is the current of the LED, which is estimated from the voltage of the LED ($V_{LED} = V - V_{CNT}$) and the UI curve of the LED.

4.7. Measurements of Peeling Force. 1-layer, 3-layer, 5-layer, and 7-layer ACNT sheets on a single-sided tape, 1-layer ACNT sheets on a stretchable tape, a pure single-sided tape, and a pure stretchable tape were prepared with an overall size of 17 × 10 mm (width × length). First, a copper tape with the same width was prepared and attached to the skin. Then each sample was loaded on the copper tape with the skin-sample area controlled to be 17 × 8 mm. The peeling force on the skin was measured by following the 90°-peeling test (Figure S12A) using the high-precision force sensor.

4.8. Monitoring of Human Electrophysiological Signals. The ACNT sheets on single-sided tapes and Ag/AgCl commercial electrodes (Ambu WhiteSensor 40713, Ambu Australia, Warriewood, Australia, or Kendall 200 series foam electrodes, Cardinal Health, Australia) were placed in different positions to measure contact impedance and ECG, EMG, and EEG signals (Figure S15). For measuring contact impedance, the interelectrode distance between a pair of electrodes was 2 cm. The impedance was measured via an LCR-6002 (GW Instek). Human electrophysiological signals (ECG, EMG, and EEG) were sampled continuously using a 16-channel analog-to-digital data acquisition system (PowerLab 16/35; AD Instruments, Bella Vista, Australia) at 2000 Hz and amplified using an ML138 Octal Bio Amp (AD Instruments, Bella Vista, Australia). Data were filtered, recorded, and analyzed using LabChart v8.1.2 software (ADInstruments, Bella Vista, Australia). MATLAB was used to estimate the later data, such as the root-mean-square of EMG signals or the STFT of EEG signals.

4.9. Monitoring ECG Signals during Artifacts from Hand Grip Exercise. The participant was asked to perform a hand grip exercise while monitoring the ECG signals (as shown in Figure S15B below). The participant was asked to perform two types of exercises. The first is to keep the participant's MVC at 50% and change the frequency (low artifact). The second is to maintain a MVC of 60% with repeated 2 s hand contractions alternated with 2 s of relaxation until fatigue (intense artifact).

4.10. Degradable and Reusable Characterizations. PDMS was used in the reusable experiment. The precursor and curing agent were mixed in a ratio of 10:1 w/w. The doctor blade method was used to create a thin layer of the mixture on a clean acrylic surface. Then the sample was placed in a desiccator for 30 min to remove bubbles. Afterward, the sample was put in an oven and heated at 120 °C for 10 min to obtain a thin, flexible PDMS layer (approximately 100 μm thick).

For reuse demonstration, a 1-layer or a 5-layer ACNT sheet on a PVA substrate was brought in contact with a PDMS layer, with the ACNT sheet sandwiched between the two polymers. Then, the sample was placed in water. Gently stirring the water yielded the detachment of PVA, leaving the ACNT sheet to remain on the PDMS (Movie S5). The sheet on PDMS was taken out of the water and left under ambient conditions for drying for one day. Then, two copper wires were connected to the 5-layer ACNT sheet on PDMS through conductive paste (silver epoxy). The sample was loaded on the home-built linear motor to examine its electrical characteristics under stretching and bending deformations.

The degradability of ACNT sheets on PVA was studied using three samples: two 1-layer ACNT sheets and one 5-layer ACNT sheet. One of the 1-layer sheets was larger than those of the other 1-layer and 5-layer sheets. A liquid chlorine solution containing 13% NaClO (Hy-Clor 5 L liquid chlorine, Bunnings, Australia) was used to degrade those sheets. After all the samples were immersed in the solution, the mixture was stirred for a few minutes to break the ACNT sheets and the PVA substrate. Then, the larger 1-layer sheet was left intact at room temperature (about 25 °C) for degradation observation. The other one-layer sheet and five-layer sheet were degraded by stirring the solution at 1500 rpm and heating to about 60 °C. The temperature was measured by a thermocouple. Stirring and heat were maintained in the daytime, while the two sheets were left intact at room temperature overnight (almost 18 h) (Figure S27).

4.11. Morphology Characterization. The morphology of a 1-layer CNT sheet was scanned by an AFM atomic force microscope (MultiMode 8-HR, Bruker) at three different positions. An optical microscope (integrated into the AFM) was used to capture images of drawn ACNT sheets with different layers and images of the prestrained ACNT sheet. An electronic digital thickness gauge of 0−10 mm (0.01 mm/0.005″) was used to estimate the thickness of the single-sided tape, the thickness of the PDMS layer, and the height of the CNT forest used for drawing ACNT sheets.

4.12. Experiments on Human Subjects. All experiments were conducted under approval from the Human Research Ethics

https://doi.org/10.1021/acsami.3c13541
ACS Appl. Mater. Interfaces 2023, 15, 58746−58760

Committees (HRECs) at the University of Southern Queensland in Australia (number: H22REA036).

■ ASSOCIATED CONTENT

Supporting Information

The Supporting Information is available free of charge at https://pubs.acs.org/doi/10.1021/acsami.3c13541.

Explanation of the electrical robustness of ACNT sheets under deformations; illustration of the fabrication process; photos of damaged ACNT sheets after being transferred from copper or aluminum films; photos of the fragility of ACNT sheets; AFM images of a 1-layer ACNT sheet; photos of deformed ACNT sheets with the skin; electrical stability of ACNT sheets under deformations; photos of prestrained ACNT sheets and their electrical responses to stretching; peeling force test; locations of placing ACNT sheets to examine contact impedance and to monitor ECG, EMG, and EEG; HRs during rest and exercise; root-mean-square values of EMG signals; EEG signals obtained using commercial electrodes; photos of reused ACNT sheets transferred from a PVA substrate to a PDMS substrate; photos and electrical responses of the reused ACNT sheets during stretching and bending; photos of degrading ACNT sheets under heating and stirring conditions; and comparison with previous work (PDF)

Movie S1 and drawing ACNT sheets from a CNT forest (MOV)

Movie S2 and fragility test of an ACNT sheet on either a nonadhesive substrate or an adhesive substrate (MOV)

Movie S3 and deformation test of ACNT sheets (MOV)

Movie S4 and stretching prestrained and nonprestrained ACNT sheets to change a LED state (MOV)

Movie S5 and shifting ACNT sheets from PVA substrates to PDMS substrates for reusability (MOV)

■ AUTHOR INFORMATION

Corresponding Authors

Duy Van Nguyen − *School of Engineering, University of Southern Queensland, Brisbane 4300 Queensland, Australia; Centre for Future Materials, University of Southern Queensland, Brisbane 4300 Queensland, Australia;* orcid.org/0000-0002-3420-2378; Email: duyvan.nguyen@usq.edu.au

Toan Dinh − *School of Engineering, University of Southern Queensland, Brisbane 4300 Queensland, Australia; Centre for Future Materials, University of Southern Queensland, Brisbane 4300 Queensland, Australia*; Email: toan.dinh@usq.edu.au

Authors

Dean Mills − *School of Health and Medical Sciences, University of Southern Queensland, Brisbane 4305 Queensland, Australia*

Canh-Dung Tran − *School of Engineering, University of Southern Queensland, Brisbane 4300 Queensland, Australia;* orcid.org/0000-0002-1011-4226

Thanh Nguyen − *School of Engineering, University of Southern Queensland, Brisbane 4300 Queensland, Australia; Centre for Future Materials, University of Southern Queensland, Brisbane 4300 Queensland, Australia;* orcid.org/0000-0002-3213-6178

Hung Nguyen − *School of Engineering, University of Southern Queensland, Brisbane 4300 Queensland, Australia; Centre for Future Materials, University of Southern Queensland, Brisbane 4300 Queensland, Australia;* orcid.org/0000-0001-9887-3691

Thi Lap Tran − *School of Engineering, University of Southern Queensland, Brisbane 4300 Queensland, Australia; Centre for Future Materials, University of Southern Queensland, Brisbane 4300 Queensland, Australia*

Pingan Song − *Centre for Future Materials, University of Southern Queensland, Brisbane 4300 Queensland, Australia;* orcid.org/0000-0003-1082-652X

Hoang-Phuong Phan − *School of Mechanical and Manufacturing Engineering, The University of New South Wales, Sydney 1466 New South Wales, Australia;* orcid.org/0000-0002-1724-5667

Nam-Trung Nguyen − *Queensland Micro- and Nanotechnology Centre, Griffith University, Brisbane 4111 Queensland, Australia*

Dzung Viet Dao − *Queensland Micro- and Nanotechnology Centre, Griffith University, Brisbane 4111 Queensland, Australia; Griffith School of Engineering, Griffith University, Gold Coast 4125 Queensland, Australia;* orcid.org/0000-0002-6348-0879

John Bell − *Centre for Future Materials, University of Southern Queensland, Brisbane 4300 Queensland, Australia*

Complete contact information is available at: https://pubs.acs.org/10.1021/acsami.3c13541

Author Contributions

The manuscript was written through the contributions of all authors. Conceptualization: D.V.N. and T.D. Methodology: D.V.N., D.M., T.N., H.N., and T.L.T. Software: D.V.N, D.M., and T.D. Resources: D.M., C.-D.T., and T.D. Validation: C.-D.T., P.S., H-P.P., N-.T.N., D.V.D., J.B., and T.D. Writing—original draft: D.V.N. Writing—review and editing: all. All authors have given approval to the final version of the manuscript.

Notes

The authors declare no competing financial interest.

■ ACKNOWLEDGMENTS

This research was supported by an Australian Government Research Training Program (RTP) Scholarship. T. Dinh acknowledges the support of Australian Research Council (ARC) projects (DE210100852 and DP240102230).

■ REFERENCES

(1) Bayoumy, K.; Gaber, M.; Elshafeey, A.; Mhaimeed, O.; Dineen, E. H.; Marvel, F. A.; Martin, S. S.; Muse, E. D.; Turakhia, M. P.; Tarakji, K. G.; Elshazly, M. B. Smart wearable devices in cardiovascular care: where we are and how to move forward. *Nat. Rev. Cardiol.* **2021**, *18* (8), 581−599.

(2) Wu, H.; Yang, G.; Zhu, K.; Liu, S.; Guo, W.; Jiang, Z.; Li, Z. Materials, Devices, and Systems of On-Skin Electrodes for Electrophysiological Monitoring and Human-Machine Interfaces. *Adv. Sci.* **2021**, *8* (2), 2001938.

(3) Kireev, D.; Sel, K.; Ibrahim, B.; Kumar, N.; Akbari, A.; Jafari, R.; Akinwande, D. Continuous cuffless monitoring of arterial blood pressure via graphene bioimpedance tattoos. *Nat. Nanotechnol.* **2022**, *17* (8), 864−870.

(4) Ates, H. C.; Nguyen, P. Q.; Gonzalez-Macia, L.; Morales-Narváez, E.; Guder, F.; Collins, J. J.; Dincer, C. End-to-end design of wearable sensors. *Nat. Rev. Mater.* **2022**, *7* (11), 887−907.
(5) Koo, J. H.; Jeong, S.; Shim, H. J.; Son, D.; Kim, J.; Kim, D. C.; Choi, S.; Hong, J. I.; Kim, D. H. Wearable Electrocardiogram Monitor Using Carbon Nanotube Electronics and Color-Tunable Organic Light-Emitting Diodes. *ACS Nano* **2017**, *11* (10), 10032−10041.
(6) Niu, S. M.; Matsuhisa, N.; Beker, L.; Li, J. X.; Wang, S. H.; Wang, J. C.; Jiang, Y. W.; Yan, X. Z.; Yun, Y. J.; Burnett, W.; Poon, A. S. Y.; Tok, J. B. H.; Chen, X. D.; Bao, Z. N. A wireless body area sensor network based on stretchable passive tags. *Nat. Electron.* **2019**, *2* (8), 361−368.
(7) Liu, S. Y.; Rao, Y. F.; Jang, H.; Tan, P.; Lu, N. S. Strategies for body-conformable electronics. *Matter* **2022**, *5* (4), 1104−1136.
(8) Leng, Z. W.; Zhu, P. C.; Wang, X. C.; Wang, Y. F.; Li, P. S.; Huang, W.; Li, B. C.; Jin, R.; Han, N. N.; Wu, J.; Mao, Y. C. Sebum-Membrane-Inspired Protein-Based Bioprotonic Hydrogel for Artificial Skin and Human-Machine Merging Interface. *Adv. Funct. Mater.* **2023**, *33*, 2211056.
(9) Jeong, J. W.; Yeo, W. H.; Akhtar, A.; Norton, J. J. S.; Kwack, Y. J.; Li, S.; Jung, S. Y.; Su, Y. W.; Lee, W.; Xia, J.; Cheng, H. Y.; Huang, Y. G.; Choi, W. S.; Bretl, T.; Rogers, J. A. Materials and Optimized Designs for Human-Machine Interfaces Via Epidermal Electronics. *Adv. Mater.* **2013**, *25* (47), 6839−6846.
(10) Ershad, F.; Thukral, A.; Yue, J.; Comeaux, P.; Lu, Y.; Shim, H.; Sim, K.; Kim, N. I.; Rao, Z.; Guevara, R.; Contreras, L.; Pan, F.; Zhang, Y.; Guan, Y. S.; Yang, P.; Wang, X.; Wang, P.; Wu, X.; Yu, C. Ultra-conformal drawn-on-skin electronics for multifunctional motion artifact-free sensing and point-of-care treatment. *Nat. Commun.* **2020**, *11* (1), 3823.
(11) Lin, M. Y.; Hu, H. J.; Zhou, S.; Xu, S. Soft wearable devices for deep-tissue sensing. *Nat. Rev. Mater.* **2022**, *7* (11), 850−869.
(12) Kabiri Ameri, S.; Ho, R.; Jang, H. W.; Tao, L.; Wang, Y. H.; Wang, L.; Schnyer, D. M.; Akinwande, D.; Lu, N. S. Graphene Electronic Tattoo Sensors. *ACS Nano* **2017**, *11* (8), 7634−7641.
(13) Kim, D. H.; Lu, N. S.; Ma, R.; Kim, Y. S.; Kim, R. H.; Wang, S. D.; Wu, J.; Won, S. M.; Tao, H.; Islam, A.; Yu, K. J.; Kim, T. I.; Chowdhury, R.; Ying, M.; Xu, L. Z.; Li, M.; Chung, H. J.; Keum, H.; McCormick, M.; Liu, P.; Zhang, Y. W.; Omenetto, F. G.; Huang, Y. G.; Coleman, T.; Rogers, J. A. Epidermal Electronics. *Science* **2011**, *333* (6044), 838−843.
(14) Yang, S.; Chen, Y. C.; Nicolini, L.; Pasupathy, P.; Sacks, J.; Su, B.; Yang, R.; Sanchez, D.; Chang, Y. F.; Wang, P.; Schnyer, D.; Neikirk, D.; Lu, N. "Cut-and-Paste" Manufacture of Multiparametric Epidermal Sensor Systems. *Adv. Mater.* **2015**, *27* (41), 6423−6430.
(15) Xu, B.; Akhtar, A.; Liu, Y.; Chen, H.; Yeo, W. H.; Park, S. I.; Boyce, B.; Kim, H.; Yu, J.; Lai, H. Y.; Jung, S.; Zhou, Y.; Kim, J.; Cho, S.; Huang, Y.; Bretl, T.; Rogers, J. A. An Epidermal Stimulation and Sensing Platform for Sensorimotor Prosthetic Control, Management of Lower Back Exertion, and Electrical Muscle Activation. *Adv. Mater.* **2016**, *28* (22), 4462−4471.
(16) Norton, J. J. S.; Lee, D. S.; Lee, J. W.; Lee, W.; Kwon, O.; Won, P.; Jung, S. Y.; Cheng, H. Y.; Jeong, J. W.; Akce, A.; Umunna, S.; Na, I.; Kwon, Y. H.; Wang, X. Q.; Liu, Z. J.; Paik, U.; Huang, Y. G.; Bretl, T.; Yeo, W. H.; Rogers, J. A. Soft, curved electrode systems capable of integration on the auricle as a persistent brain-computer interface. *Proc. Natl. Acad. Sci. U.S.A.* **2015**, *112* (13), 3920−3925.
(17) Yang, S. X.; Chen, Y. C.; Nicolini, L.; Pasupathy, P.; Sacks, J.; Su, B.; Yang, R.; Sanchez, D.; Chang, Y. F.; Wang, P. L.; Schnyer, D.; Neikirk, D.; Lu, N. S. "Cut-and-Paste" Manufacture of Multiparametric Epidermal Sensor Systems. *Adv. Mater.* **2015**, *27* (41), 6423−6430.
(18) Li, B. M.; Yildiz, O.; Mills, A. C.; Flewwellin, T. J.; Bradford, P. D.; Jur, J. S. Iron-on carbon nanotube (CNT) thin films for biosensing E-Textile applications. *Carbon* **2020**, *168*, 673−683.
(19) Zhu, Z. J.; Guo, S. Z.; Hirdler, T.; Eide, C.; Fan, X. X.; Tolar, J.; McAlpine, M. C. 3D Printed Functional and Biological Materials on Moving Freeform Surfaces. *Adv. Mater.* **2018**, *30* (23), 1707495.
(20) Zhang, L. W.; Wang, X.; Xu, W. Z.; Zhang, Y. Y.; Li, Q. W.; Bradford, P. D.; Zhu, Y. T. Strong and Conductive Dry Carbon Nanotube Films by Microcombing. *Small* **2015**, *11* (31), 3830−3836.
(21) Bulmer, J. S.; Kaniyoor, A.; Elliott, J. A. A Meta-Analysis of Conductive and Strong Carbon Nanotube Materials. *Adv. Mater.* **2021**, *33* (36), No. e2008432.
(22) (a) Goh, G. L.; Agarwala, S.; Yeong, W. Y. Directed and on-demand alignment of carbon nanotube: a review toward 3D printing of electronics. *Adv. Mater. Interfaces* **2019**, *6* (4), 1801318. (b) Meyyappan, M. *Carbon Nanotubes: Science and Applications*; CRC Press, 2004.
(23) Guo, Y.; Shi, E.; Zhu, J.; Shen, P. C.; Wang, J.; Lin, Y.; Mao, Y.; Deng, S.; Li, B.; Park, J. H.; Lu, A. Y.; Zhang, S.; Ji, Q.; Li, Z.; Qiu, C.; Qiu, S.; Li, Q.; Dou, L.; Wu, Y.; Zhang, J.; Palacios, T.; Cao, A.; Kong, J. Soft-lock drawing of super-aligned carbon nanotube bundles for nanometre electrical contacts. *Nat. Nanotechnol.* **2022**, *17* (3), 278−284.
(24) Zhang, M.; Fang, S. L.; Zakhidov, A. A.; Lee, S. B.; Aliev, A. E.; Williams, C. D.; Atkinson, K. R.; Baughman, R. H. Strong, transparent, multifunctional, carbon nanotube sheets. *Science* **2005**, *309* (5738), 1215−1219.
(25) Chetyrkina, M. R.; Fedorov, F. S.; Nasibulin, A. G. In vitrotoxicity of carbon nanotubes: a systematic review. *RSC Adv.* **2022**, *12* (25), 16235−16256.
(26) (a) Ferrari, L. M.; Sudha, S.; Tarantino, S.; Esposti, R.; Bolzoni, F.; Cavallari, P.; Cipriani, C.; Mattoli, V.; Greco, F. Ultraconformable Temporary Tattoo Electrodes for Electrophysiology. *Adv. Sci.* **2018**, *5* (3), 1700771. (b) Zhang, L.; Kumar, K. S.; He, H.; Cai, C. J. Y.; He, X.; Gao, H. X.; Yue, S. Z.; Li, C. S.; Seet, R. C. S.; Ren, H. L.; Ouyang, J. Y. Fully organic compliant dry electrodes self-adhesive to skin for long-term motion-robust epidermal biopotential monitoring. *Nat. Commun.* **2020**, *11* (1), 4683.
(27) (a) Zhang, S. P.; Chhetry, A.; Zahed, M. A.; Sharma, S.; Park, C.; Yoon, S.; Park, J. Y. On-skin ultrathin and stretchable multifunctional sensor for smart healthcare wearables. *npj Flexible Electron.* **2022**, *6* (1), 11. (b) Sun, B. H.; McCay, R. N.; Goswami, S.; Xu, Y. D.; Zhang, C.; Ling, Y.; Lin, J.; Yan, Z. Gas-Permeable, Multifunctional On-Skin Electronics Based on Laser-Induced Porous Graphene and Sugar-Templated Elastomer Sponges. *Adv. Mater.* **2018**, *30* (50), 1804327.
(28) Kim, J. H.; Kim, S. R.; Kil, H. J.; Kim, Y. C.; Park, J. W. Highly Conformable, Transparent Electrodes for Epidermal Electronics. *Nano Lett.* **2018**, *18* (7), 4531−4540.
(29) Tran, C. D.; Humphries, W.; Smith, S. M.; Huynh, C.; Lucas, S. Improving the tensile strength of carbon nanotube spun yarns using a modified spinning process. *Carbon* **2009**, *47* (11), 2662−2670.
(30) Yang, Z. B.; Chen, T.; He, R. X.; Guan, G. Z.; Li, H. P.; Qiu, L. B.; Peng, H. S. Aligned Carbon Nanotube Sheets for the Electrodes of Organic Solar Cells. *Adv. Mater.* **2011**, *23* (45), 5436−5439.
(31) Di, J. T.; Hu, D. M.; Chen, H. Y.; Yong, Z. Z.; Chen, M. H.; Feng, Z. H.; Zhu, Y. T.; Li, Q. W. Ultrastrong, Foldable, and Highly Conductive Carbon Nanotube Film. *ACS Nano* **2012**, *6* (6), 5457−5464.
(32) Kozono, M.; Sato, H. Resistance change characteristics of spray-deposited carbon nanotube thin film with bending deformation. *Jpn. J. Appl. Phys.* **2020**, *59*, SGGH07.
(33) Barnett, C. J.; Evans, C.; McCormack, J. E.; Gowenlock, C. E.; Dunstan, P.; Wade Adams; Orbaek White, A.; Barron, A. R. Experimental measurement of angular and overlap dependence of conduction between carbon nanotubes of identical chirality and diameter. *Nano Lett.* **2019**, *19* (8), 4861−4865.
(34) Wang, Y. J.; Li, M.; Gu, Y. Z.; Zhang, X. H.; Wang, S. K.; Li, Q. W.; Zhang, Z. G. Tuning carbon nanotube assembly for flexible, strong and conductive films. *Nanoscale* **2015**, *7* (7), 3060−3066.
(35) Zhang, Z. L.; Innocent, M. T.; Tang, N.; Li, R. Y.; Hu, Z. X.; Zhai, M.; Yang, L. J.; Ma, W. J.; Xiang, H. X.; Zhu, M. F. Electromechanical Performance of Strain Sensors Based on Viscoelastic Conductive Composite Polymer Fibers. *ACS Appl. Mater. Interfaces* **2022**, *14* (39), 44832−44840.

(36) Nguyen, T.; Dinh, T.; Dau, V.; Tran, C. D.; Phan, H. P.; Nguyen, T. K.; Nguyen, H. K.; Riduan, F. A.; Guzman, P.; Nguyen, N. T.; Dao, D. V. A Wearable, Bending-Insensitive Respiration Sensor Using Highly Oriented Carbon Nanotube Film. *IEEE Sens. J.* **2021**, *21* (6), 7308−7315.
(37) Xu, F.; Wang, X.; Zhu, Y. T.; Zhu, Y. Wavy Ribbons of Carbon Nanotubes for Stretchable Conductors. *Adv. Funct. Mater.* **2012**, *22* (6), 1279−1283.
(38) Liu, D. J.; Zhu, P. C.; Zhang, F. K.; Li, P. S.; Huang, W. H.; Li, C.; Han, N. N.; Mu, S. R.; Zhou, H.; Mao, Y. C. Intrinsically stretchable polymer semiconductor based electronic skin for multiple perceptions of force, temperature, and visible light. *Nano Res.* **2023**, *16* (1), 1196−1204.
(39) Yao, S. S.; Ren, P.; Song, R. Q.; Liu, Y. X.; Huang, Q. J.; Dong, J. Y.; O'Connor, B. T.; Zhu, Y. Nanomaterial-Enabled Flexible and Stretchable Sensing Systems: Processing, Integration, and Applications. *Adv. Mater.* **2020**, *32* (15), 1902343.
(40) Yang, G. G.; Zhu, K. H.; Guo, W.; Wu, D. R.; Quan, X. L.; Huang, X.; Liu, S. Y.; Li, Y. Y.; Fang, H.; Qiu, Y. Q.; Zheng, Q. Y.; Zhu, M. L.; Huang, J.; Zeng, Z. G.; Yin, Z. P.; Wu, H. Adhesive and Hydrophobic Bilayer Hydrogel Enabled On-Skin Biosensors for High-Fidelity Classification of Human Emotion. *Adv. Funct. Mater.* **2022**, *32* (29), 2200457.
(41) Hermens, H. J.; Freriks, B.; Disselhorst-Klug, C.; Rau, G. Development of recommendations for SEMG sensors and sensor placement procedures. *J. Electromyogr. Kinesiol.* **2000**, *10* (5), 361−374.
(42) (a) Chi, Y. M.; Jung, T. P.; Cauwenberghs, G. Dry-Contact and Noncontact Biopotential Electrodes: Methodological Review. *IEEE Rev. Biomed. Eng.* **2010**, *3*, 106−119. (b) Spach, M. S.; Barr, R. C.; Havstad, J. W.; Long, E. C. Skin-electrode impedance and its effect on recording cardiac potentials. *Circulation* **1966**, *34* (4), 649−656.
(43) Yamamoto, Y.; Yamamoto, D.; Takada, M.; Naito, H.; Arie, T.; Akita, S.; Takei, K. Efficient Skin Temperature Sensor and Stable Gel-Less Sticky ECG Sensor for a Wearable Flexible Healthcare Patch. *Adv. Healthcare Mater.* **2017**, *6* (17), 1700495.
(44) Wang, L. F.; Liu, J. Q.; Yang, B.; Yang, C. S. PDMS-Based Low Cost Flexible Dry Electrode for Long-Term EEG Measurement. *IEEE Sens. J.* **2012**, *12* (9), 2898−2904.
(45) Kalevo, L.; Miettinen, T.; Leino, A.; Kainulainen, S.; Korkalainen, H.; Myllymaa, K.; Toyras, J.; Leppanen, T.; Laitinen, T.; Myllymaa, S. Effect of Sweating on Electrode-Skin Contact Impedances and Artifacts in EEG Recordings With Various Screen-Printed Ag/Agcl Electrodes. *IEEE Access* **2020**, *8*, 50934−50943.
(46) Kusayama, T.; Wong, J. S.; Liu, X.; He, W. B.; Doytchinova, A.; Robinson, E. A.; Adams, D. E.; Chen, L. S.; Lin, S. F.; Davoren, K.; Victor, R. G.; Cai, C.; Dai, M. Y.; Tian, Y.; Zhang, P.; Ernst, D.; Rho, R. H.; Chen, M. L.; Cha, Y. M.; Walega, D. R.; Everett, T. H.; Chen, P. S. Simultaneous noninvasive recording of electrocardiogram and skin sympathetic nerve activity (neuECG). *Nat. Protoc.* **2020**, *15* (5), 1853−1877.
(47) (a) Ochs, A.; Nippes, M.; Salatzki, J.; Weberling, L. D.; Riffel, J.; Muller-Hennessen, M.; Giannitsis, E.; Osman, N.; Stehning, C.; Andre, F.; Katus, H. A.; Frey, N.; Friedrich, M. G.; Ochs, M. M. Dynamic Handgrip Exercise: Feasibility and Physiologic Stress Response of a Potential Needle-Free Cardiac Magnetic Resonance Stress Test. *Front. Cardiovasc. Med.* **2021**, *8*, 755759. (b) Lewis, S. F.; Taylor, W. F.; Bastian, B. C.; Graham, R. M.; Pettinger, W. A.; Blomqvist, C. G. Haemodynamic responses to static and dynamic handgrip before and after autonomic blockade. *Clin. Sci.* **1983**, *64* (6), 593−599.
(48) Laughlin, M. H. Cardiovascular response to exercise. *Am. J. Physiol.* **1999**, *277* (6), S244.
(49) Wang, L.; Lu, N. S. Conformability of a Thin Elastic Membrane Laminated on a Soft Substrate With Slightly Wavy Surface. *J. Appl. Mech.* **2016**, *83* (4), 041007.
(50) Fang, H.; Wang, L.; Fu, Z. Z.; Xu, L.; Guo, W.; Huang, J.; Wang, Z. L.; Wu, H. Anatomically Designed Triboelectric Wristbands with Adaptive Accelerated Learning for Human-Machine Interfaces. *Adv. Sci.* **2023**, *10* (6), 2205960.
(51) (a) Nishihara, K.; Isho, T. Location of electrodes in surface EMG. *EMG Methods for Evaluating Muscle and Nerve Function*; IntechOpen, 2012. (b) De Luca, C. J. The use of surface electromyography in biomechanics. *J. Appl. Biomech.* **1997**, *13* (2), 135−163.
(52) Xu, Y.; Zhao, G.; Zhu, L.; Fei, Q.; Zhang, Z.; Chen, Z.; An, F.; Chen, Y.; Ling, Y.; Guo, P.; Ding, S.; Huang, G.; Chen, P. Y.; Cao, Q.; Yan, Z. Pencil-paper on-skin electronics. *Proc. Natl. Acad. Sci. U.S.A.* **2020**, *117* (31), 18292−18301.
(53) Barry, R. J.; De Blasio, F. M. EEG differences between eyes-closed and eyes-open resting remain in healthy ageing. *Biol. Psychol.* **2017**, *129*, 293−304.
(54) Yang, L.; Gan, L.; Zhang, Z.; Zhang, Z.; Yang, H.; Zhang, Y.; Wu, J. Insight into the Contact Impedance between the Electrode and the Skin Surface for Electrophysical Recordings. *ACS Omega* **2022**, *7* (16), 13906−13912.
(55) Lin, Y. X.; Cao, Y.; Ding, S. J.; Zhang, P. P.; Xu, L.; Liu, C. C.; Hu, Q. L.; Jin, C. H.; Peng, L. M.; Zhang, Z. Y. Scaling aligned carbon nanotube transistors to a sub-10 nm node. *Nat. Electron.* **2023**, *6* (7), 506−515.
(56) Moya, A.; Gabriel, G.; Villa, R.; Javier del Campo, F. Inkjet-printed electrochemical sensors. *Curr. Opin. Electrochem.* **2017**, *3* (1), 29−39.
(57) (a) Sinha, A. K.; Goh, G. L.; Yeong, W. Y.; Cai, Y. Ultra-Low-Cost, Crosstalk-Free, Fast-Responding, Wide-Sensing-Range Tactile Fingertip Sensor for Smart Gloves. *Adv. Mater. Interfaces* **2022**, *9* (21), 2200621. (b) Fisher, C.; Skolrood, L. N.; Li, K.; Joshi, P. C.; Aytug, T. Aerosol-Jet Printed Sensors for Environmental, Safety, and Health Monitoring: A Review. *Adv. Mater.* **2023**, *8*, 2300030.
(58) Tay, R. Y.; Song, Y.; Yao, D. R.; Gao, W. Direct-ink-writing 3D-printed bioelectronics. *Mater. Today* **2023**.
(59) Ashammakhi, N.; Hernandez, A. L.; Unluturk, B. D.; Quintero, S. A.; de Barros, N. R.; Hoque Apu, E.; Bin Shams, A.; Ostrovidov, S.; Li, J.; Contag, C.; et al. Biodegradable implantable sensors: materials design, fabrication, and applications. *Adv. Funct. Mater.* **2021**, *31* (49), 2104149.
(60) (a) Hosseini, E. S.; Dervin, S.; Ganguly, P.; Dahiya, R. Biodegradable Materials for Sustainable Health Monitoring Devices. *ACS Appl. Bio Mater.* **2021**, *4* (1), 163−194. (b) Brown, M. S.; Somma, L.; Mendoza, M.; Noh, Y.; Mahler, G. J.; Koh, A. Upcycling Compact Discs for Flexible and Stretchable Bioelectronic Applications. *Nat. Commun.* **2022**, *13* (1), 3727.
(61) Dinh, T.; Nguyen, T.; Phan, H. P.; Nguyen, T. K.; Dau, V. T.; Nguyen, N. T.; Dao, D. V. Advances in Rational Design and Materials of High-Performance Stretchable Electromechanical Sensors. *Small* **2020**, *16* (14), No. e1905707.
(62) Nguyen, T. K.; Dinh, T.; Phan, H. P.; Tran, C. D.; Foisal, A. R. M.; Zhu, Y.; Dao, D. V. Electrically Stable Carbon Nanotube Yarn Under Tensile Strain. *IEEE Electron Device Lett.* **2017**, *38* (9), 1331−1334.
(63) (a) Yu, Y.; Luo, Y.; Guo, A.; Yan, L.; Wu, Y.; Jiang, K.; Li, Q.; Fan, S.; Wang, J. Flexible and transparent strain sensors based on super-aligned carbon nanotube films. *Nanoscale* **2017**, *9* (20), 6716−6723. (b) Zhang, C.; Li, H.; Huang, A.; Zhang, Q.; Rui, K.; Lin, H.; Sun, G.; Zhu, J.; Peng, H.; Huang, W. Rational design of a flexible CNTs@ PDMS film patterned by bio-inspired templates as a strain sensor and supercapacitor. *Small* **2019**, *15* (18), 1805493.
(64) (a) Zhu, P. C.; Zhang, B. S.; Wang, H. Y.; Wu, Y. H.; Cao, H. J.; He, L. B.; Li, C. Y.; Luo, X. P.; Li, X.; Mao, Y. C. 3D printed triboelectric nanogenerator as self-powered human-machine interactive sensor for breathing-based language expression. *Nano Res.* **2022**, *15* (8), 7460−7467. (b) Dinh, T.; Nguyen, T.; Phan, H. P.; Nguyen, N. T.; Dao, D. V.; Bell, J. Stretchable respiration sensors: Advanced designs and multifunctional platforms for wearable physiological monitoring. *Biosens. Bioelectron.* **2020**, *166*, 112460.
(65) (a) Chen, M.; Qin, X.; Zeng, G. Biodegradation of Carbon Nanotubes, Graphene, and Their Derivatives. *Trends Biotechnol* **2017**,

35, 836−846. (b) Yang, M.; Zhang, M. Biodegradation of Carbon Nanotubes by Macrophages. *Front Mater.* **2019**, *6*, 225.
(66) Zhang, M. F.; Deng, Y. M.; Yang, M.; Nakajima, H.; Yudasaka, M.; Iijima, S.; Okazaki, T. A Simple Method for Removal of Carbon Nanotubes from Wastewater Using Hypochlorite. *Sci. Rep.* **2019**, *9*, 1284.
(67) Zhang, M. F.; Yang, M.; Nakajima, H.; Yudasaka, M.; Iijima, S.; Okazaki, T. Diameter-Dependent Degradation of 11 Types of Carbon Nanotubes: Safety Implications. *ACS Appl. Nano Mater.* **2019**, *2* (7), 4293−4301.
(68) Dahiya, R.; Gottardi, G.; Laidani, N. PDMS residues-free micro/macrostructures on flexible substrates. *Microelectron. Eng.* **2015**, *136*, 57−62.

https://doi.org/10.1021/acsami.3c13541
ACS Appl. Mater. Interfaces 2023, 15, 58746−58760